



SPE 90861

Rotary Sidewall Cores- A Cost Effective Means of Determining Young's Modulus

Larry K. Britt and Michael B. Smith, NSI Technologies, Inc., Ziad Haddad, Devon Energy Corporation, Jennifer Reese, BP, and Patrick Kelly, BP-Canada Energy Company

Copyright 2004, Society of Petroleum Engineers Inc.

This paper was prepared for presentation at the SPE Annual Technical Conference and Exhibition held in Houston, Texas, U.S.A., 26–29 September 2004.

This paper was selected for presentation by an SPE Program Committee following review of information contained in a proposal submitted by the author(s). Contents of the paper, as presented, have not been reviewed by the Society of Petroleum Engineers and are subject to correction by the author(s). The material, as presented, does not necessarily reflect any position of the Society of Petroleum Engineers, its officers, or members. Papers presented at SPE meetings are subject to publication review by Editorial Committees of the Society of Petroleum Engineers. Electronic reproduction, distribution, or storage of any part of this paper for commercial purposes without the written consent of the Society of Petroleum Engineers is prohibited. Permission to reproduce in print is restricted to a proposal of not more than 300 words; illustrations may not be copied. The proposal must contain conspicuous acknowledgment of where and by whom the paper was presented. Write Librarian, SPE, P.O. Box 833836, Richardson, TX 75083-3836, U.S.A., fax 01-972-952-9435.

Abstract

The objective of hydraulic fracturing is to design and execute a fracture stimulation treatment that achieves the desired fracture dimensions (length and conductivity) to maximize a well's production rate and reserve recovery. To achieve this objective, there are several critical parameters to the process, and these fall into two distinct categories: 1) parameters over which we have little control, but need to understand, and 2) those that we control, but have lesser impact on the process. The first category includes fracture height, fluid loss coefficient, tip effects, and Young's modulus. The second category includes pump rate and fluid viscosity. Of the former parameters, Young's Modulus is the only variable that can be measured, in advance, via lab tests.

Traditionally, Young's Modulus is measured through stress-strain testing of geologic samples (core plugs) which always demanded an L/d (Length/ diameter) ratio of at least 2:1. The reason for this criterion is that the ultimate failure mechanism for most rocks under compression loads is the formation of a shear fracture. For most rock types, this shear fracture will form at an angle of about 30° from the axis of the maximum compression load. Thus, a 2:1 L/d ratio allows a through-going shear fracture to form for a failure angle of 30°. For stress-strain testing NOT concerned with ultimate failure of the sample, this valid criterion has always been followed – arbitrarily and artificially. Unfortunately, this sample criterion generally eliminates the use of sidewall cores.

This paper details and documents an evaluation of the Length to diameter criteria through finite element modeling, tri-axial compression testing of aluminum, and compression testing of actual sedimentary rock samples. Through this work, it is evident that core samples of L/d significantly less

than 2:1 can provide reliable values of static Young's Modulus. Further, these results indicate that rotary sidewall cores can be utilized to determine Young's Modulus in many applications provided adequate sample quality assurance is undertaken to ensure sample integrity.

Introduction

Determination of mechanical rock properties is important to the oil and gas industry for reservoir compaction, borehole stability, formation control, and hydraulic fracturing. Measurements of the elastic rock properties have historically been conducted on whole core and via wireline measurements once the wellbore has been drilled. Application of these methods at the well site in real time on drill cuttings and with Measurement While Drilling (MWD) to improve or optimize the drilling process is the focus of much ongoing research¹⁻⁵. Studies by Ringstad et al², Zausa et al³, and Santarelli et al⁴ evaluated the use of drill cuttings for mechanical properties determination. Because of this, these studies focused on sample size sensitivities and determined that the micro indentation measurements correlated well to Uniaxial Compressive Strength of the rock. However, these measurements correlated poorly with Young's Modulus or porosity.

Similarly, Nes et al⁵ investigated sample size sensitivities on both the static and dynamic behavior of the Pierre Shale. This study evaluated the elastic properties of 0.39 inch diameter samples 0.16 inches in length ($L/d = 0.4$) and found that the static Young's Moduli of the "hard" shale samples was in excellent agreement (i.e. within 3.5 %) with larger sized core plugs. The static Young's Moduli of the soft shale samples tested were in much poorer agreement (i.e. nearly a 20 % error) as compared to larger sized samples tested. Finally, this work showed excellent agreement (i.e. +/- 2 %) between the dynamic moduli determined with a Continuous Wave Technique (CWT used on smaller samples) and a Pulse Transmission Technique (used on larger samples).

Many studies^{6-10 & 13} have compared the static and dynamic elastic properties and developed correlations. All found the dynamic Young's Modulus to be as much as twice as large as the static Young's Modulus. These studies also identified index parameters for improving the correlations. For example, Yale et al⁶ developed a correlation of dynamic to static Young's Modulus with correlation coefficients, R^2 , of 0.79, 0.73, and 0.68 for lithologic indices of limestone, dolomitic

cemented siltstones, and siltstones and mudstones, respectively.

Similarly, Tuman et al⁷ showed static and dynamic measurements from saturated sandstone core samples from the Carbondale, Berea, Boise, and Torpedo Formations. The correlation coefficient reported for the Carbondale and Berea data was 0.868. Morales et al⁸, and Farquhar et al⁹ established good correlations of dynamic to static Young's Modulus using porosity as the primary geomechanical index or indicator.

The effect of Young's Modulus on the fracturing process has been reviewed by several authors. Rahim and Holditch¹⁰ investigated the effect of Young's Modulus on fracture geometry and the resultant fracture dimensions.

Smith et al¹¹ investigated the effect of Young's Modulus on fracture width and net treating pressure. In this study, the effect of Young's Modulus on fracture width was physically measured with a downhole closed circuit television camera while bottom hole treating pressure data was measured and used to validate the fracture geometry assumption of Perkins and Kern (modified to account for fracture growth into zones of higher stress). The coupling of the television and bottom hole pressure measurement resulted in a dramatic visualization of the importance of Young's Modulus on fracture width and fracture geometry as the net treating pressure in this well increased to a critical pressure of 450 psi where the net pressure flattened. Subsequently, the net treating pressure fell as the fracture height more than doubled from 54 to 110 feet.

Lacy¹² showed the value of determining the Young's Modulus on fracture design to achieve optimized fracture dimensions. This study presented a large amount of static and dynamic Young's Modulus data and showed that the dynamic Young's Modulus was nearly twice the static Young's Modulus. Thus, using static measurements for fracture optimization and design is paramount.

The application of static Young's Modulus in the fracture design, execution, and post appraisal process is important to achieving the desired post fracture dimensions. The application of this data is limited by core availability. The objective of this work is to:

- 1) Demonstrate the value of laboratory measurements of elastic properties to the hydraulic fracturing process,
- 2) Establish a Length to diameter (L/d) criteria for measurement of elastic properties in core through finite element modeling, non-failure triaxial compression testing of calibrated aluminum (homogeneous material) and sedimentary rock (heterogeneous material),
- 3) Validate the use of and establish methods and procedures for triaxial compression testing of rotary sidewall cores,
- 4) Establish quality assurance guidelines for core measurements of elastic properties, and in particular for elastic measurement of properties through triaxial compression testing of rotary sidewall core.
- 5) Demonstrate the value of this data through case studies of the Upper Wilcox Formation in South Texas.

Discussion

Rock Mechanics for Fracturing

The objective of hydraulic fracturing is to design and execute a fracture treatment that will achieve the desired fracture dimensions (length and conductivity) to maximize a wells production rate and reserves. To achieve this objective, there are several critical parameters to the process. These parameters fall into two distinct categories, those over which we have little control, but need to understand, and those that we control, but have lesser impact on the process. The former category includes fracture height, fluid loss coefficient, fracture tip effects, and Young's modulus. The latter category includes pump rate and fluid viscosity.

The importance and interaction of these categories is best understood by reviewing fracture-modeling relations including both fracture geometry and material balance. For confined height fractures, for example, net pressure, fracture width, and shut-in pressure decline relations are shown in equation 1.

$$p_{net} = (p - \sigma_c) \propto \left[\frac{E^4}{H^4} \left(\frac{\mu Q x_f}{E} \right) + \frac{K_{lc-app}^4}{H^2} \right]^{1/4}$$

$$w \propto \left[\left(\frac{\mu Q x_f}{E} \right) + \frac{K_{lc-app}^4 H^2}{E^4} \right]^{1/4} \quad \dots \dots (1)$$

$$\Delta P^* \propto \frac{E^4 C H_p}{H^2}$$

where: ΔP^* is the pressure decline parameter from pressure decline analysis, and is related to the rate of pressure decline. This clearly shows that modulus is a very important, even critical parameter to all phases of fracture behavior!

As shown, the net pressure is directly related to fracture height and nearly so to modulus. Also, note the limited role of viscosity, pump rate, and fracture length on net pressure. Young's Modulus is also a dominant parameter in determining fracture width. Finally, modulus affects the pressure decline behavior, and thus the analysis of pressure decline data for the critical parameter, fluid loss coefficient, C.

Similarly, net pressure behavior for a radial fracture is shown in equation 2 below. Once again the importance of modulus on the fracturing process is highlighted.

$$p_{net} = (p - \sigma_c) \propto \left[\frac{E^4}{R^4} \left(\frac{\mu Q R}{E} \right) + \frac{K_{lc-app}^4}{R^2} \right]^{1/4} \quad \dots \dots (2)$$

Interestingly, even for a Gertsma deKlerk model where fracture length is the critical parameter, net treating pressure and width are still nearly directly controlled by modulus.

These relations show that net treating pressure and thus fracture geometry are controlled by fracture height and modulus. Fracture height is generally controlled by in-situ stresses and is difficult to directly measure. Fluid loss, "C", is a complex function of the fracturing and reservoir fluids, formation relative permeability, fluid loss additives, etc., thus

"C" must be measured by field tests – but analysis of these tests depends on modulus! Finally, tip effects, $K_{k\text{-app}}$, is poorly understood and difficult to measure directly. Thus, the ONLY variable subject to routine measurement from lab tests is modulus. Certainly definitive data for modulus is required before sensible use can be made of sophisticated fully 3-D fracture geometry models!

Plain Strain Modulus

Note that the modulus needed in hydraulic fracturing and represented in equations 1 and 2 is the plain strain modulus, E' . Equation 3 shows the relationship between the plain strain modulus and Young's modulus, E , and Poisson's Ratio, v . As shown, Poisson's Ratio has little impact on the plain strain modulus because in hydrocarbon bearing rocks Poisson's Ratio generally only varies from 0.2 to 0.3.

$$E' = E / (1 - v^2) \quad \dots \dots \dots (3)$$

Determination of Elastic Properties

Dynamic Measurements

Sonic Logs

The modulus important to fracturing is the static linear elastic rock property. Many in the industry have attempted to use the Young's Modulus determined from acoustic logs. The modulus determined in this manner represents a dynamic value, and nearly always differs greatly from static lab measurements. In fact, variations between static and dynamic modulus of a factor of two are common, and even larger variations have been reported. Further, the dynamic modulus is always greater than static modulus, and since modulus directly controls P_{Net} and fracture geometry, significant errors in these predictions can result by utilizing a dynamic modulus from logs.

A dynamic Young's Modulus can be calculated from compressional travel times without requiring shear wave data. As a result, dynamic properties can be calculated from conventional Borehole Compensated sonic logs. Dipole or full waveform sonic logs with both shear and compressional travel time data is acceptable although unnecessary.

Ultrasonic Tests

Dynamic moduli can be derived from ultrasonic measurement in the lab. In this approach, compressional velocity, V_p , and shear velocity, V_s , are measured with a Pulse Transmission technique with nominal velocities of 300-500 KHz. Bulk density of each core sample is measured and the Young's Modulus, E , Shear Modulus, and Poisson's Ratio, v , calculated from the following equations.

$$S_{\text{dynamic}} = \rho * \frac{13,400,000,000}{V_s} \quad \dots \dots \dots (4)$$

$$v_{\text{dynamic}} = \frac{(0.5)(V_s^2 - 2 * V_p^2)}{(V_s^2 - V_p^2)} \quad \dots \dots \dots (5)$$

$$E_{\text{dynamic}} = 2 * S_{\text{dynamic}} * (1 + v_{\text{dynamic}}) \quad \dots \dots \dots (6)$$

Ultrasonic Test Procedures

The procedures for conducting laboratory shear and compressional velocity tests are, for the most part, relatively standardized. The assembled sample and instrumentation fixtures are installed in a pressure vessel. After this, typical procedures might include the following steps:

- The core plugs are cleaned, evacuated, and allowed to come to thermal and vapor equilibrium with the atmosphere.
- The sample is then saturated with 25,000 ppm NaCl brine under a pressure of 1,000 psi for 12 hours.
- The samples are then placed in a pressure vessel, confining pressure and pore pressure increased to 250 psi for five minutes and then released.
- Velocities are measured using the Pulse Transmission technique. The nominal frequency of the measurements is 500 KHz for the compressional wave velocity and 350 KHz for the shear wave velocity.

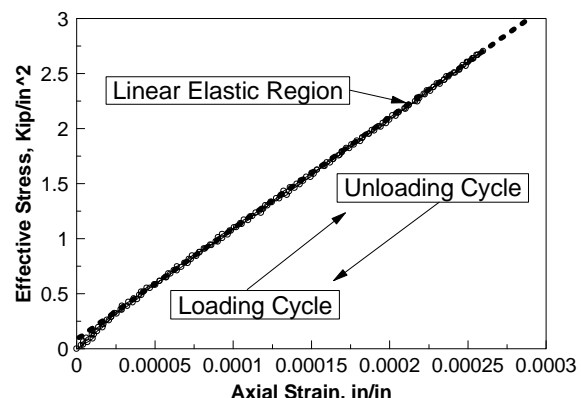
Static Measurements

Triaxial Compression Tests

Triaxial compression testing is used to measure Young's modulus (E) and Poisson's ratio (v). In a conventional test, a cylindrical core sample having a 2 to 1 length to diameter ratio is loaded axially at a constant confining pressure. In addition to axial stress, the axial and lateral strains are monitored during the test and used to determine E and v .

Figure 1 plots axial and lateral strain for a triaxial compression test of a carbonate core sample. Note, that axial strain is linear throughout nearly all of the loading/unloading cycle. This sample was not taken to failure and showed no evidence

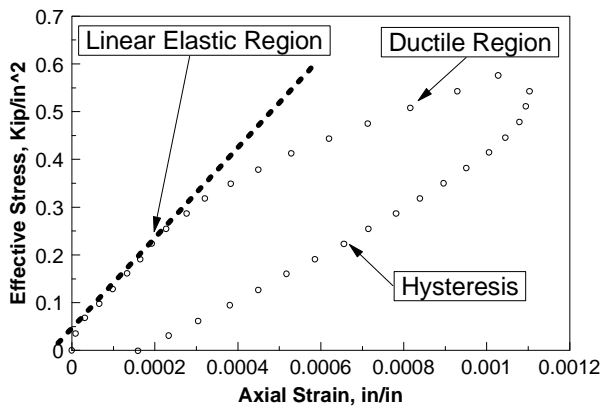
Figure 1: Hard Rock Triaxial Compression Test



of destruction of the internal rock fabric. The slope of the linear portion of the axial strain curve represents the linear elastic constant, Young's modulus. In this example, the Young's modulus was determined to be 11.0×10^6 psi. Poisson's ratio is determined by a ratio of average lateral strain over average axial strain. For the sample in Figure 1 the Poisson's ratio was determined to be 0.32.

Figure 2 shows a plot of axial and lateral strains for a triaxial compression test of an unconsolidated core sample. As shown, the unconsolidated rock sample has a linear elastic region during the loading cycle of the compression test.

Figure 2: Unconsolidated Rock Triaxial Compression Test



However, at some part the poorly cemented fabric of the sample begins to rearrange or deform. This ductile region, though not a catastrophic failure of the sample, does represent permanent deformation of the core plug. As a result, when the sample is unloaded a hysteresis is exhibited where the unloading cycle does not track the stress-strain behavior of the loading cycle.

Recognize that generally all core samples during destructive compression testing have ductile behavior. In hard rock, however, the ductile region occurs at or very near the confined compressive strength of the sample (failure point) and therefore is not always evident. Since ductile failure in soft poorly consolidated rock occurs prior to the development of a through-going shear fracture and collection of rotary sidewall cores in such rock is seldom done due to risks associated with sticking tools the application of these results may be limited. However, even in poorly consolidated rocks, the results of this L/d analysis are applicable provided sample quality is assured.

Triaxial Compression Test Procedures

Instrumentation for the triaxial compression tests consists of applying an axial load with a servo-controlled actuator. Confining pressure and pore pressure are hydraulically generated. Axial forces are applied to the core samples. Axial stress is monitored with a load cell. Confining pressure and pore pressure are monitored with conventional pressure transducers. Axial and radial strains are measured using strain extensometers.

The cylindrical core samples are cut to a length-to-diameter ratio of two (2:1) with an inert fluid and endground flat and parallel, in accordance to ISRM standards

(recommended tolerance in end parallelism is ± 0.001 inches). Each sample is installed between hardened steel endcaps and this assembly is sealed with a thin, deformable, heat shrink jacketing material. The jacket prevents confining fluid from penetrating into the sample and allows independent control and monitoring of the confining and pore pressures during testing. The endcaps are ported to allow application of pore pressure and/or flow if permeability is measured.

The procedures for conducting a triaxial compression test are relatively standardized. The assembled sample and instrumentation fixtures are installed in a pressure vessel.

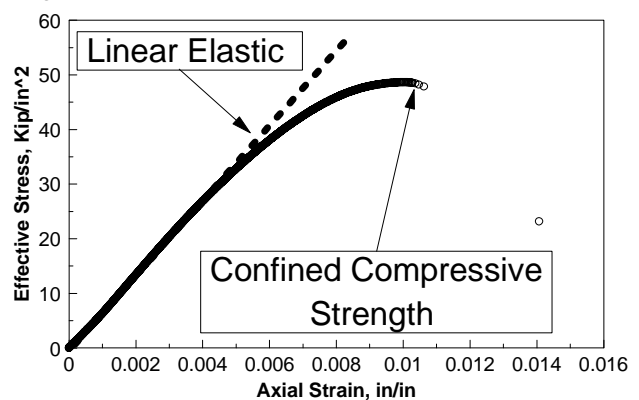
- Fill the pressure vessel with hydraulic confining fluid. Raise the confining pressure to a nominal value (100 psi) at a servo-controlled rate (1 psi/s). This initial confining pressure is applied so that there will always be at least a small difference between confining pressure acting outside of the jacket and pore pressure in the rock (inside the jacket). Otherwise leakage will occur.
- The axial stress difference is increased at a rate corresponding to an axial strain rate of $10^{-5}/\text{s}$. Alternatively, rather than controlling the axial strain rate, the axial stress rate can be controlled.
- The sample is unloaded slowly, the pressure vessel is emptied and the sample assembly is disassembled.

Further Application of Triaxial Compression Data

In addition to determining the basic elastic constants of Young's modulus and Poisson's Ratio, triaxial compression testing can also be utilized to determine the confined compressive strength of the sample. If triaxial compression testing is performed at several confining pressures and coupled with unconfined compression and tensile test data, a representative failure envelope can be constructed and used to estimate formation failure.

Figure 3 shows a plot of axial and lateral strains for a triaxial compression test of a consolidated sandstone core sample. As shown, this sample was loaded axially to failure at

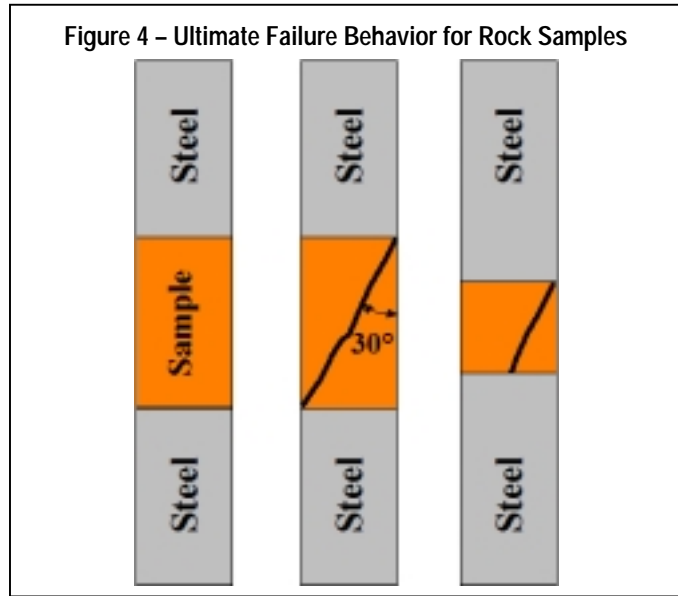
Figure 3: Hard Rock Triaxial Compression Test to Failure



a constant confining pressure. Also note the small deviation from the linear elastic region prior to failure. This represents the ductile region of the sample as described previously. Note, determination of the confined compressive strength requires the samples to be failed and is, therefore, subject to the L/d limitation of 2:1.

Sample Dimension Considerations

Traditionally, stress-strain testing of geologic samples has always demanded an L/d (Length/ diameter) ration of at least “2”. The reason for this is illustrated in Figure 4. The ultimate failure, i.e., total failure, mechanism for most rocks under compression loads is the formation of a shear fracture. For most rock types, this shear fracture will form at an angle of about 30° from the axis of the maximum compression load. Thus, a 2:1 L/d ratio allows a through-going shear fracture to form for a failure angle of 30°. As illustrated, the use of a shorter sample (relative to the diameter) results in constraining the development of this shear fracture, thus, artificially making the sample appear “stronger”. For stress-strain testing NOT concerned with ultimate failure of the sample, this valid criterion has always been followed – arbitrarily and artificially as seen in the discussion below.



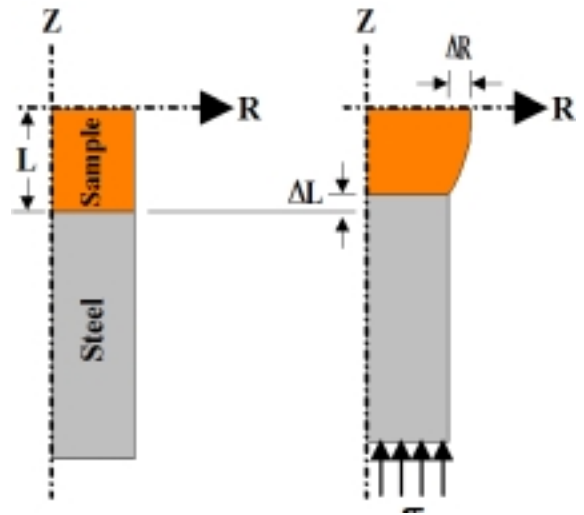
Stress-Strain Testing for Elastic Properties

For rocks under small-load, small-strain stress conditions, there will be minimal change in the internal fabric of the rock (grain rearrangement, grain cracking, etc.), and for most rock types, the deformation can be accurately described as “elastic”. That is, the relation between stress and strain can be described using a “Young’s modulus” and “Poisson’s Ratio”. Since sample failure in any form, let alone the total failure

associated with a through going shear fracture, is NOT of interest, the rigorous insistence of a 2:1 L/d ratio may not be necessary. However, there still can be concerns with the L/d ratio as illustrated in Figure 5.

This figure illustrates 1/4 of a typical sample. That is, the sample is assumed radially symmetric about the “Z” axis, and symmetric about the middle of the sample. Thus, the figure represents the bottom, right-hand portion of the sample. As the sample is loaded, friction between the steel loading platen along the bottom of the sample will, in general, NOT let the rock sample expand (due to Poisson’s Ratio effects), as it

Figure 5 – FEM Modeling of Rock Stress-Strain Test

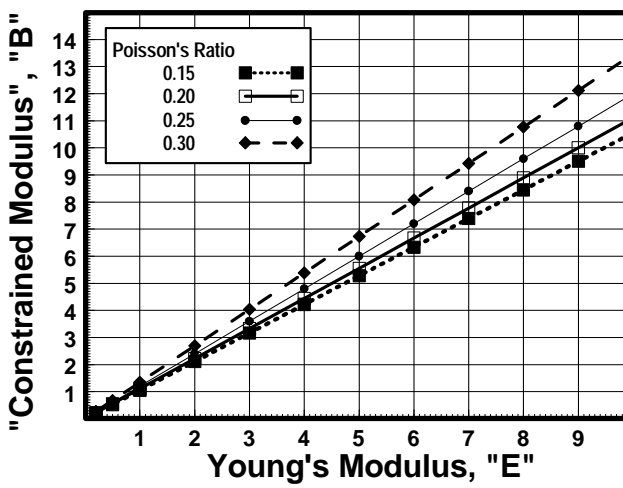


should. That is, the steel loading platens are essentially “rigid” in comparison to most rock. This will tend to “stiffen” the sample, and for some small L/d the test may yield an erroneously high value for Young’s modulus.

Theoretical Limit

As L/d approaches “0”, eventually a situation will arise for NO lateral expansion of the rock sample can occur during the compression. This is, in fact, a particular type of test known as a “Uniaxial Strain Test”. In such tests, the sample is compressed while simultaneously applying lateral confining pressure to prevent lateral expansion, and the stress-strain ratio measured in such a test is termed the “Constrained modulus”, “B”. “B” can be related to Young’s modulus and Poisson’s Ratio by

$$B = E \frac{1-\nu}{(1+\nu)(1-2\nu)} \quad \dots\dots\dots(7)$$

Figure 6 – Relation Between "B" and "E"

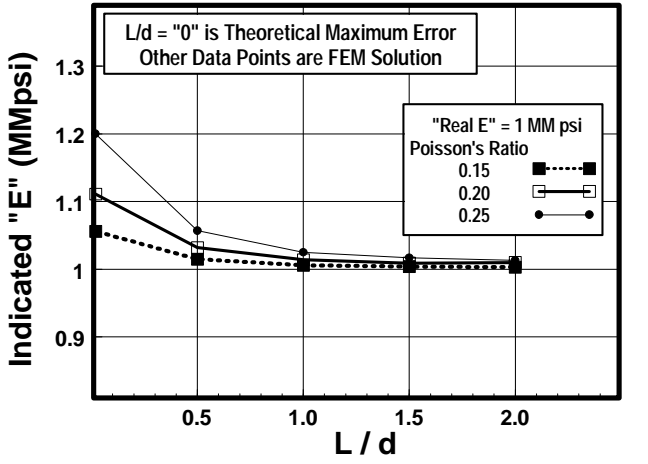
and the relation between "B" and "E" is plotted in Figure 6.

Thus, for some (probably very short) L/d ratio, a stress-strain test will actually be measuring "B". If this is mistakenly identified as Young's modulus, "E", the resulting value for "E" will be too high by as much as 20 to 30%. This is, of course, a worst case error since: a) the steel platens are not completely rigid, and b) it would probably require a very small L/d before true uniaxial strain conditions would prevail. Still, the "exact" allowable L/d ration is not known.

Finite Element Modeling

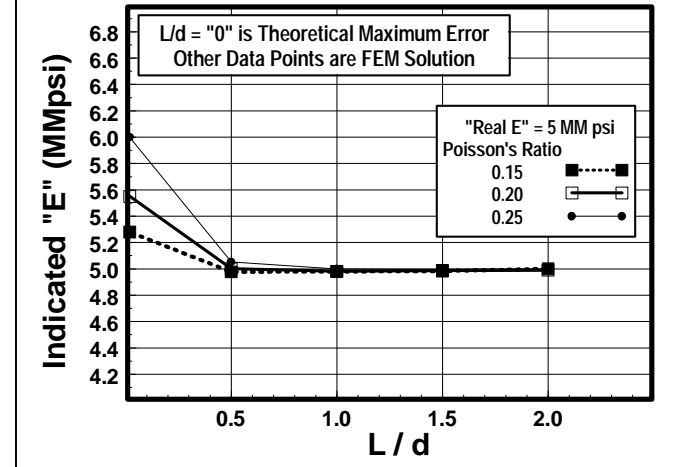
As illustrated in Figure 5, a FEM (finite element method) model was constructed for a typical test sample. The model included 1-½ of steel platen compressing the rock sample. A uniform stress was applied to the bottom of the steel platen, and the resulting compression (ΔL) and radial expansion (ΔR) was recorded and used to calculate the "indicated" values for Young's modulus/Poisson's Ratio. FEM models were then run for varying values of "E" and "v" for the rock sample, and the results were somewhat surprising, but very definitive.

Figure 7 plots the results (for a rock sample "E" of 1×10^6 psi)

Figure 7 – Possible Modulus Error Vs. L/d (E=1x10⁶ psi)

psi and varying values of "v") for L/d ratios from 0.5 to 2. As seen, the error for an L/d ratio of "1" is down into the range of typical experimental error (1 to 2%), and thus, samples of this dimension should be acceptable. Under special conditions, probably even samples with L/d < 1 could be acceptable.

This behavior was also checked for varying values of "E" for the rock sample, and it was found that overall behavior was similar for any value. That is, the "error" illustrated in Figure 7 can almost just be considered as a "percent" error. As an example, Figure 8 plots similar calculations for a case where the "E" for the rock sample was assumed to be 5×10^6 psi.

Figure 8 – Possible Modulus Error Vs. L/d (E=5x10⁶ psi)

Poisson's Ratio

Results of the FEM modeling for Poisson's Ratio were similar. For all cases, the "indicated" value for "v" was within 1% of the actual value for L/d ≥ 1 .

Aluminum Calibration Tests

The next phase of the L/d investigation was to conduct

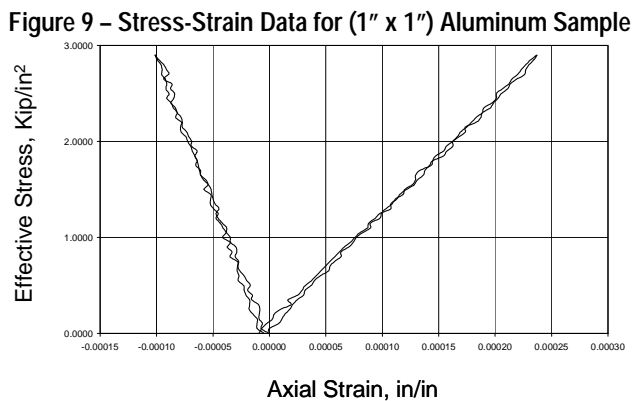
Table 1 – Rock & Material Properties (Aluminum 2024-T351)

| Component/Property | Weight % |
|----------------------------|-----------|
| Al | 93.5 |
| Cr | < 0.1 |
| Cu | 3.8 – 4.9 |
| Fe | < 0.5 |
| Mg | 1.2 – 1.8 |
| Mn | 0.3 – 0.9 |
| Si | < 0.5 |
| Ti | < 0.15 |
| Zn | < 0.25 |
| Modulus of Elasticity, GPa | 72.4 + 2% |
| Poisson's Ratio | 0.33 |

experimental triaxial compression tests of the elastic properties for a homogeneous material of known elastic properties. Aluminum 2024-T351 was used for this purpose. This material is used to calibrate the triaxial compression test equipment and was, therefore, ideal for this purpose. Table 1 summarizes the mineral constituents and material property characteristics of aluminum 2024-T351.

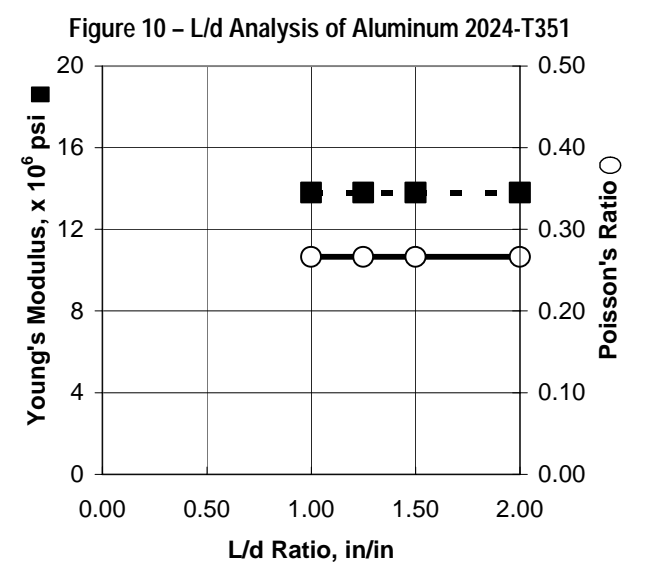
First, a sample of one inch diameter aluminum 2024-T351 was cut to a length of two inches ($L/d = 2$) with an inert fluid and the endground flat and parallel, in accordance to ISRM standards and the aluminum calibration sample was loaded in the test frame and a triaxial compression test conducted as described in the prior section on triaxial compression testing procedures.

Next, the aluminum sample was cut to 1.50", 1.25", and 1.00" in length and retested. Figure 9 shows a plot of axial and lateral strain for the triaxial compression test of the 1" x 1" aluminum sample, $L/d = 1$. Note, that axial strain is linear



throughout the entire loading and unloading cycle. Analysis of the linear elastic region of the plot describes a Young's Modulus of 10.65×10^6 psi and a Poisson's Ratio of 0.345. In fact, all of the tests conducted on the aluminum samples provided the same results independent of confining pressure.

Figure 10 shows a plot of the Young's Modulus and Poisson's Ratio as a function of the L/d Ratio. As shown, the



elastic property results for the aluminum 2024-T351 were independent of L/d ratio from a 1:1 to a 2:1. Note, triaxial compression tests of the aluminum 2024-T351 for even smaller L/d ratios was limited by the load frame configuration used in the triaxial testing. Without this limitation, it is anticipated that similar results would be realized at L/d ratios of 0.5 to 1 as indicated by the finite element modeling. In any event, the application to core plugs with an L/d ratio of at least 1:1 appears viable.

Triaxial Tests on Sedimentary Rock

It is now obvious that the L/d ratio can be relaxed when testing homogeneous samples given the results of the finite element modeling and aluminum calibration tests. But how do we apply these results to samples that are less than homogeneous and in some instances quite heterogeneous on the core plug scale.

To address this issue in greater detail triaxial compression tests were conducted on actual sedimentary rock samples. Whole core plugs with L/d ratios of 2:1 were taken from the Upper Wilcox Formation in South Texas and highly laminated sand/silt/shale strata from the Western Canadian Sedimentary Basin. The test procedure was similar to the aluminum calibration tests, in that, a triaxial compression test was conducted for each sample with an $L/d = 2$ at confining pressure. Subsequent to this test, the sample was cut down to an L/d of 1.5:1 and retested.

Upper Wilcox Formation

First, let's look at the results from the Upper Wilcox Formation. Table 2 summarizes the mineralogical composition of three Upper Wilcox Formation sand samples where the L/d

Table 2 – Mineralogical Characterization Of Upper Wilcox

| Constituent | Sample | | |
|-------------------------------------|---------------|------|------|
| | 1 | 2 | 3 |
| Quartz | 66 | 73 | 62 |
| CaCO₃ | 3 | 30 | 4 |
| Dolomite | 5 | 4 | 5 |
| Illite | 7 | 8 | 8 |
| Smectite | 0 | 0 | 8 |
| Kaolinite | 0 | 0 | 0 |
| Chlorite | 4 | 3 | 3 |
| Pyrite | 0 | 0 | 1 |
| Ortho | 4 | 3 | 3 |
| Oligio | 3 | 4 | 2 |
| Mixed | 5 | 3 | 0 |
| Albite | 0 | 0 | 0 |
| Anhydrite | 0 | 0 | 1 |
| Siderite | 3 | 2 | 3 |
| API Units | 23 | 25 | 23 |
| E_{static} (L/d=2.0) | 3.51 | 3.38 | 4.11 |
| E_{static} (L/d=1.5) | 3.44 | 3.40 | 4.25 |
| Measurement Error, % | 1.99 | 0.59 | 3.29 |

evaluation was conducted. A review of this table shows that though the three samples were identified as predominately sands (GR response and quartz content) there are great differences in their mineralogical make-up. For example, sample 2 has nearly eight to ten times the calcium carbonate present as the other samples. Further, sample 3 has nearly twice the amount of clay components as the other samples tested.

Also shown in the table are the results of the Young's Modulus testing for each sample and L/d ratio. As shown, extremely small errors in Young's Modulus between 0.59 and 3.29 percent were seen by reducing the sample size from an L/d of 2:1 to an L/d of 1.5:1. One final and important thought about this analysis is that it is interesting that the sample with the greatest amount of clay constituents had the largest (although still small) error in Young's Modulus. Is this error the result of the L/d ratio and heterogeneity effect or are these results an artifact of the validation procedure. That is are we introducing error in the analysis by loading and unloading, cutting the samples, and loading and unloading the samples again. If this is the case, it would be plausible that the sample with the greatest clay content would be most susceptible to this effect.

Figure 11 shows a plot of effective stress versus axial strain for the loading and unloading cycles for both L/d ratios (L/d = 2 and L/d = 1.5) tested in sample 3. Analysis of this

Figure 11: Stress-Strain Plot for Sample 3 (L/d = 2 & 1.5)

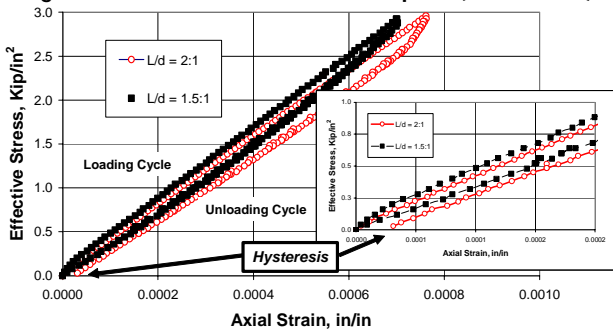


figure shows that even though the difference in the Young's Modulus (i.e. slope of linear elastic region of the loading cycle) between the two L/d ratios is extremely small, the difference likely results from the validation procedure itself. As shown, the loading and unloading cycles of the initial test (L/d = 2) under confining pressure differs indicating hysteresis occurred. That is, the rock fabric was altered, however slightly, during the initial test. As a result, it is surprising that the elastic modulus difference was only 3.29 percent. A similar comparison of the other samples stress-strain curves indicated that no ductile like hysteresis occurred as seen here. Finally, the ductility of sample 3 (Figure 11) may be due to the increased clay content of the sample. It should be noted, however, that this ductile behavior can be eliminated or at least limited by better controlling the test and monitoring how far we go up the stress-strain curve before we unload the sample. Once linear elastic behavior is seen how much linear data is required to determine a Young's Modulus? Again, this

issue is most important in tests in shales, high clay content sands, or poorly consolidated formations.

At this point of the investigation, relaxation of the L/d ratio appears appropriate for at least homogeneous or near homogeneous sandstone samples given the maximum error encountered with the samples tested is less than four percent.

Heterogeneous Canadian Sands, Silts, and Shale

Next, highly laminated sand, silt, and shale strata from the Western Canadian Sedimentary Basin was included in the investigation to evaluate the extension/relaxation of the L/d ratio in more heterogeneous systems.

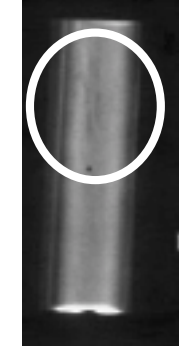
Rotary sidewall cores were being routinely obtained and evaluated in this tight formation gas reservoir in Canada. Some but limited whole core was available for both routine core analysis and rock mechanics testing. In order to develop a relationship between rotary sidewall core (routinely available), whole core, and logs (available on a foot by foot basis) a study of the effect of sample size on elastic mechanical rock properties was undertaken.

This evaluation included taking core plugs from the whole core with length to diameter (L/d) ratios of 2:1 and conducting tri-axial compression tests. Next, the samples were cut to 1.5" lengths (L/d = 1.5) and retested. Finally, the samples were cut to 1" (L/d = 1) and tested.

Five samples were evaluated in this manner. However, prior to reducing the L/d ratio of the samples, they were examined with a fluoroscope. Figure 12 shows the results of one of the fluoroscopic inspections that highlights some internal laminations that were not seen from a visual inspection of the core plug. These laminations appeared parallel to the long axis of the core as indicated.

Following the fluoroscopic inspection, triaxial compression tests for L/d ratio of 2:1 and 1.5:1 were conducted on the samples. Results of the triaxial compression tests showed differences in Young's Modulus approaching twenty percent for samples where the fluoroscopic evaluation identified significant internal features (bedding or micro-cracks) in the sample. Samples where no internal features were detected or that were identified as massive had insignificant differences in the results. For example, the sample identified in Figure 12 had a nearly twenty percent

Figure 12: Fluoroscopic Inspection of Core Plug



This core plug exhibited wavy laminations nearly parallel to the long axis of core!

Lower portion of sample appears massive!

difference between the L/d of 2:1 and L/d of 1.5:1. The differences in the measurements became greater as the L/d ratio was reduced to 1:1 for the samples with internal features.

Thus, the evaluation of the heterogenous geologic samples indicated that if features existed in the samples then fairly large differences in results could be anticipated with smaller L/d ratios. This result is not unexpected since the smaller the sample the greater the effect of any feature (scaling issue).

In addition to these highly laminated and heterogeneous sedimentary samples additional testing has been conducted on other sandstone core material. Results of this work showed differences in Young's Modulus of less than 1% for samples with an L/d of 2:1 as compared to 1.5:1. In fact, for all of the sedimentary samples tested (approximately 27) in this evaluation, the average difference between samples 2:1 to 1.5:1 is only 3.3 percent excluding the samples with internal features (based on fluoroscopic examination).

At this point of the investigation, relaxation of the L/d ratio and use of rotary sidewall cores appears appropriate for at least homogeneous or near homogeneous sandstone samples given the maximum error encountered with the samples tested is less than four percent. More heterogeneous geologic samples can be mechanically tested provided the sample quality is assured through mineralogic and fluoroscopic inspection and it is understood that larger deviations from conventional analysis of whole core plugs may result.

Sample Quality Assurance

The preceding sections of the paper have established a window of opportunity for determining elastic rock properties by conducting triaxial compression tests on rotary sidewall cores. For this to provide quality results, extreme care should be taken with the collection of the rotary core plugs, delivery to the laboratory, integrity and quality assurance of the samples, as well as development of a work plan that specifically identifies the triaxial compression test procedures for each sample.

1. Ensure careful collection and handling of the rotary sidewall core from the wellsite through the laboratory,
2. Prevent desiccation of shale samples,
3. Conduct a fluoroscopic inspection of rotary sidewall core plugs prior to conducting any mechanical properties testing,
4. Conduct mineralogical evaluation (FTIR or X-Ray Diffraction) of the sidewall core plugs, and
5. Develop a work plan for rock mechanics testing of the rotary sidewall core samples to ensure quality elastic properties result from the triaxial compression testing. Work plan should include and consider the impact of sample heterogeneity and mineralogy on the ability to determine good estimates of the elastic properties.

Static Properties from Rotary Sidewall Cores

Field Example 1: Jim Hogg County, Tx

The Upper Wilcox Formation is the predominant producing formation in South Texas. Gas production in this area of South Texas is primarily from the 5th Hinnant sand with the 2nd and 7th Hinnant sands appearing prospective. It is well understood that the objective of hydraulic fracturing in these formations is the creation of effective fracture length and conductivity to stimulate well performance. The creation of effective fracture length can be difficult with crosslinked fracturing fluids in the Upper Wilcox Formation if the bounding beds necessary to contain a large fracture have insufficient stress contrast and/or significantly lower Young's Modulus.

As previously described whole core was available for rock mechanics testing of the 5th Hinnant. However, no whole core is available from the 2nd and 7th Hinnant although rotary side wall core is available. The preceding investigation showed that core plugs with length to diameter ratios less than 2 to 1 could be utilized provided adequate quality assurance is undertaken. Relaxation of the L/d criterion and application of triaxial compression testing to rotary sidewall cores may help better understand the mechanical properties of these prospective sands.

Triaxial Compression Testing

Triaxial compression testing was performed on sand, silts, and shale core samples from the Upper Wilcox Formation to determine the static Young's Modulus. Velocity measurements were made and a dynamic to static Young's Modulus correlation developed. The triaxial compression and ultrasonic tests were conducted on rotary sidewall core plugs and the static and dynamic modulus determined, respectively.

The laboratory project consisted of triaxial compression and ultrasonic testing ten samples from the 2nd, 5th, and 7th Hinnant Formations at confining pressures of 1300, 2600, and 3900 psi. An additional five 5th Hinnant samples of sufficient length to diameter ratio (i.e. length to diameter ratio of 1.5:1.0) were identified and included in the testing for completeness. These samples were tested (i.e. triaxial compression and ultrasonic tests) at a confining pressure of 2600 psi.

It should be noted that no mineralogical tests were conducted on the sidewall core samples and visible and Scanning Electron Microscope (SEM) inspection was used to identify the presence of clays in the samples. As a result of this inspection it was determined that the 5th Hinnant sidewall core samples were clay rich and likely to destruct if the samples were hydrated prior to compression testing as is usually done. Therefore, the 5th Hinnant sidewall core samples were tested dry. Both the 2nd Hinnant and 7th Hinnant sidewall core samples were hydrated prior to triaxial compression testing, however.

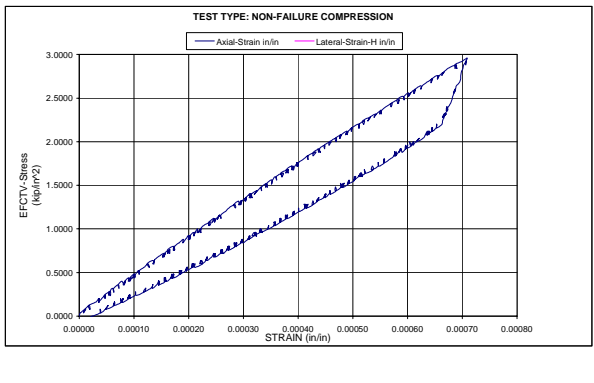
Results of this testing indicate an average Young's Modulus for the three 2nd Hinnant, nine 5th Hinnant, and three 7th Hinnant rotary sidewall core plugs at an effective confining pressure of 2,600 psi was 5.41×10^6 psi, 3.90×10^6 psi, and 3.87×10^6 psi, respectively.

These triaxial compression results indicate that the Young's Modulus for the 2nd and 7th Hinnant sands were

nearly twice the magnitude used previously in the area for fracture stimulation designs. Increasing the Young's Modulus by a factor of two will have significant impact on future fracture stimulation designs and net treating pressure analyses.

Figure 13 shows a plot of stress versus strain for the rotary

Figure 13: Stress-Strain Curve (5th Hinnant-Upper Wilcox)



sidewall core plug from the 5th Hinnant sand under a confining pressure of 2,600 psi. As shown, a linear stress strain relationship was seen indicative of elastic behavior of the sample. The interpretation of the slope of the axial strain loading indicates a Young's Modulus of 4.34×10^6 psi.

Note the chatter in the loading and unloading stress-strain data. This behavior although unusual in most compression tests commonly occurs when testing Upper Wilcox sediments. One plausible explanation for these "energy releases" is that they represent grain to grain rearrangement in the poorly sorted bioturbated Upper Wilcox sediments. Though unconfirmed, the behavior is typically only seen in the bioturbated sediments of the Upper Wilcox.

Ultrasonic Tests

In addition to the triaxial compression testing, a series of ultrasonic measurements were made. Each sample was subjected to a sonic frequency of 300 to 500 KHz in the lab and the compressional and shear velocities were measured. It should be noted that two shear travel times (i.e. S1 and S2) were measured. The second shear travel time is measured perpendicular to the first, such that, a comparison of the two shear travel times is a measure of the shear anisotropy. Comparison of the shear velocities shows little evidence of anisotropy in the sidewall core samples as most of the samples shear velocities are well within five percent of each other. On the other hand, a couple of samples from the 5th Hinnant showed a difference in the shear velocities of nine and thirteen percent, respectively, indicating some amount of shear wave anisotropy in these samples.

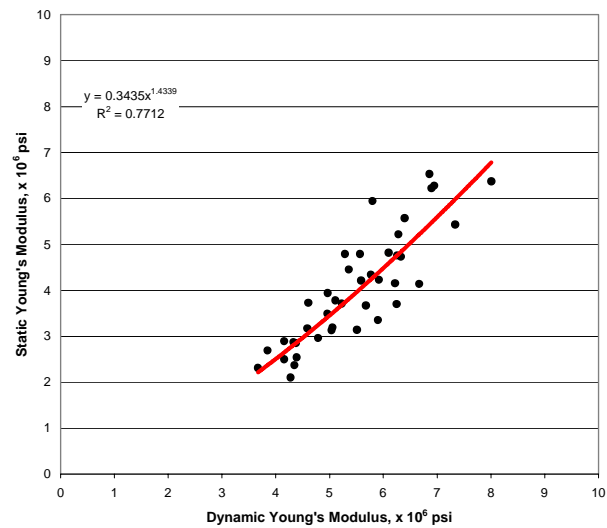
Dynamic to Static Correlations

Next, the shear and compressional velocities and the bulk density were utilized to calculate dynamic rock properties for the Upper Wilcox core samples. The dynamic Young's Modulus determined through ultrasonic testing was then compared to the static Young's Modulus determined through triaxial compression testing. This comparison, shown in

Figure 14, indicates the dynamic Modulus is always greater than the static Modulus.

Figure 14 further shows a correlation of static Young's Modulus versus dynamic Young's Modulus for all of the Upper Wilcox data collected and interpreted. As shown, an extremely good dynamic to static Young's Modulus

Figure 14: Dynamic to Static Young's Modulus Correlation



correlation with a correlation coefficient, R^2 , of 0.77 exists for the 2nd, 5th, and 7th Hinnant of the Upper Wilcox Formation. Not only does data in this correlation come from three separate horizons it also includes sandstones, siltstones, and shale test results at various confining pressures, and as mentioned previously, includes both drained and undrained test results as well as whole core and rotary sidewall core results. Given the quality of the correlation and the variability in the data set control, the use of rotary sidewall core for static elastic property measurements appears to be a viable means of populating a rock mechanics data set provided adequate quality control measures are employed (See sample quality assurance measures).

Field Example 2: Zapata County, Tx

The next case history using rotary sidewall core plugs for triaxial compression testing is also a South Texas Upper Wilcox Formation example although from Zapata County, Tx. This field example will demonstrate how rotary sidewall cores can be used in rock properties measurements of static Young's Modulus and embedment to aid in a South Texas field development. In this example, a well was drilled to the deeper of three Upper Wilcox Formation targets (i.e. deeper sand labeled the "C" sand and the shallower horizons labeled the "B", and "A" sands, respectively).

Original Well Evaluation

The well was initially completed and fracture stimulated in the "C" sand. The "C" sand in this well proved to be a poor performer, so the "C" sand was isolated and the "B" sand perforated. The "B" sand perforations produced approximately 800 mscfd unstimulated and a production log indicated behind pipe communication between the "B" and "C" sands.

The “B” sand was then fracture stimulated using 100 mesh sand in the pad to limit the behind pipe communication. Pre-frac data collection indicated that fracture height growth into the “A” sand was likely and the well was fracture stimulated making in excess of 5 mmcfpd with declining tubing pressure. Production decline analysis raised concerns about the performance of the well and speculation regarding the cause of the rapid production decline was initiated.

Proppant embedment, fracture clean-up and gel damage issues, limited drainage, and permeability reduction due to compaction were just some of the arguments postulated. Rotary sidewall core plugs were collected in an offset well in the “B” sand. Rock mechanical testing was used to improve the fracture design, execution, and understanding of the well performance.

Figure 15: Field Example 2- Gamma-Ray, Neu-Den X-Plot

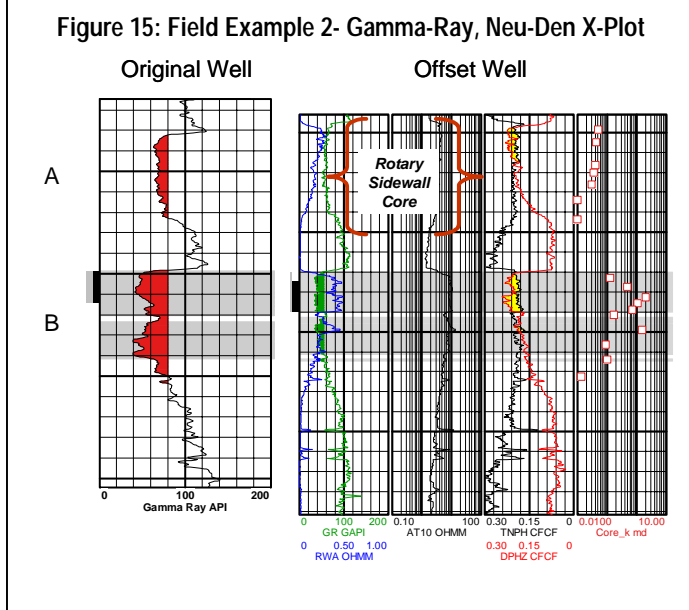


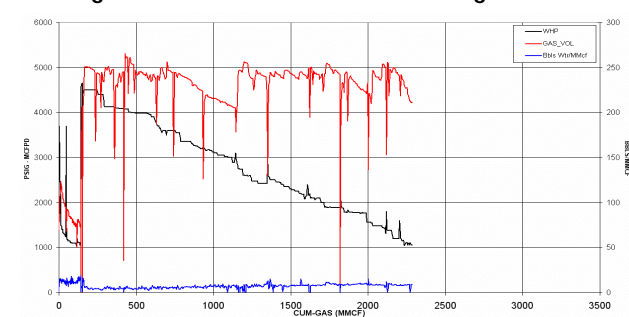
Figure 15 highlights the A and B sands in the two wells of interest to this example via a Gamma Ray, Neutron-Density Porosity Cross plot presentation. Also shown on this plot is the “A” sand interval where rotary sidewall cores were taken for subsequent rock mechanics and embedment testing.

Figure 16 shows a post fracture stimulation performance curve for the original well that raised concerns. As shown, the well produced between 4 and 5 mmcfpd (2.9 BCF) for a period of nearly eleven months with hardly any water production while the tubing pressure fell dramatically from 4,600 psi to 1,000 psi.

Post Frac Evaluation

Unconstrained (guessed at mechanical properties and permeability) post fracture history matching of the net treating pressure data indicated that the fracture of the “B” sand grew into the “A” sand, limiting the fracture half-length to 150 feet with a fracture conductivity, k_{bf} , of in excess of 200 mdft ($F_{CD} = 2.50$ for $k = 0.5$ md). It should be noted that an $F_{CD} = 2$ is optimum in permeable reservoirs where transient flow is unimportant and limited gel damage has occurred to the

Figure 16: Well Performance Curve-Original Well

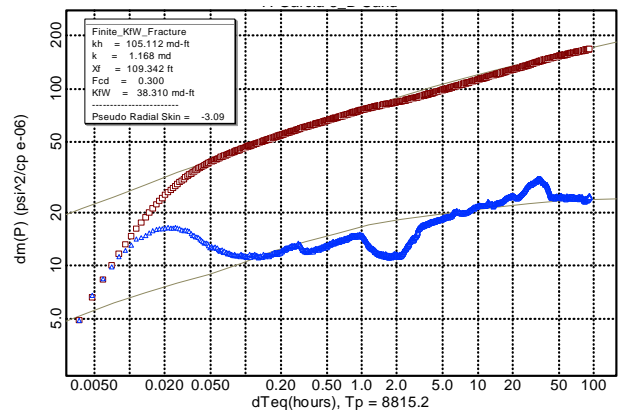


fracture. Further, studies have shown that an $F_{CD} > 10$ is necessary to ensure fracture fluid clean-up and a fully effective fracture.

Due to the concerns about the well performance in the original well and upcoming plans for a “B” sand completion in an offset well, rotary sidewall cores (reference Figure 15) were authorized in the offset and a build-up test was conducted in the original well to better constrain the mechanical properties, evaluate embedment potential, and better constrain the permeability and drainage, respectively.

Figure 17 shows the history match of the post fracture build-up test response in the original well. As shown, a

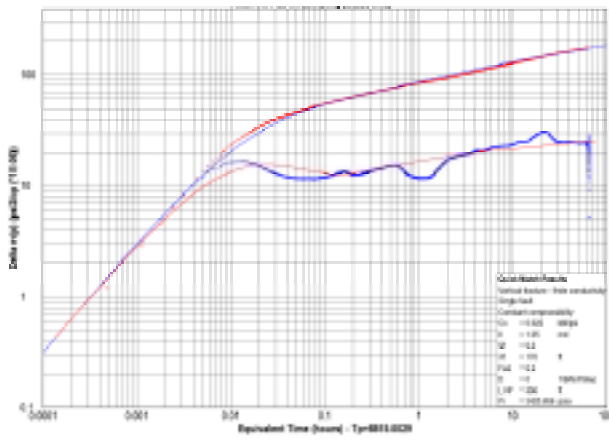
Figure 17: Post Fracture Build-Up In Original Well



fracture half-length of 170 feet (113 % of the half-length estimated in the post fracture history matching) and extremely low fracture conductivity of 60 mdft (30 % of post fracture history match). Note, the history match of this finite conductivity build-up test behavior indicated a reservoir permeability of 1.2 md (skin = -3.1). As a result, the post fracture build-up indicates a Dimensionless Fracture Capacity, F_{CD} , of 0.29 well below what is required for optimal well performance and fracture fluid clean-up. One final note about the post fracture build-up test analysis is that it suggests depletion, potentially significant depletion, has occurred since the original well was placed on production. Though the original reservoir pressure was 5,800 psi, the pressure only built to 3,425 psi during the nearly one hundred hour (4 days) test.

Next, an iterative model history match of the post fracture build-up test was performed. The purpose of this approach was to determine whether reservoir boundaries and not necessarily inadequate fracture conductivity and length are the

Figure 18: Post-Frac Build-Up, Original Well w/ 1 Sealing Fault



cause of the degrading well performance.

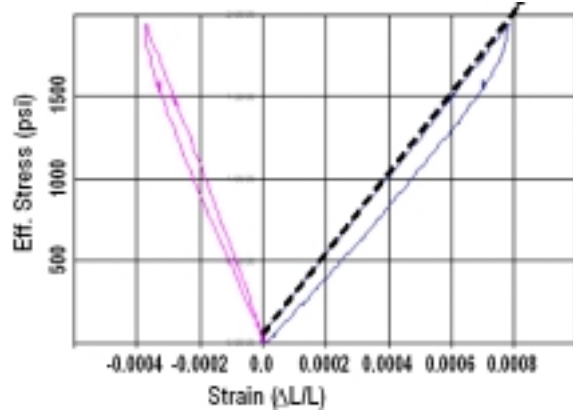
Figure 18 shows the post fracture build-up test matched in this manner. As shown, the match required a single sealing fault 350 feet from the original well. Even so, the fracture dimensions ($x_f = 170$, $k_f b_f = 60$ md, and $F_{CD} = 0.3$) are less than desired and attempts should be made to improve the fracture dimensions for the offset well.

Triaxial Compression Testing

To develop a better understanding of the mechanical rock properties of the formation, triaxial compression tests of the rotary sidewall cores were conducted employing the recommended quality assurance procedures. In addition, a series of embedment tests were conducted with both shale and sand sidewall core plugs.

Figure 19 shows an example of the resulting stress-strain data collected for one of the "A" sand rotary sidewall cores with an L/d ratio of 1.5:1. As shown, a well defined linear elastic region was identified and interpreted for static Young's Modulus. Note, that hysteresis of the loading and unloading

Figure 19: Stress-Strain Data ("A" Sand Rotary Sidewall Core)



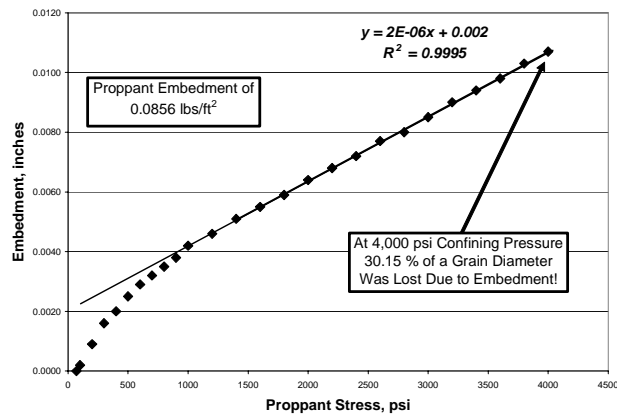
cycle was limited and that there is little sign of ductile failure of the sample. The interpreted Young's Modulus is 2.5×10^6 psi as compared to a log derived dynamic Young's Modulus of 4.4×10^6 psi.

Embedment Testing

In order to better understand the abnormal drawdown behavior an embedment test was conducted on one sand and one shale sample. The embedment test was conducted by evenly distributing the applied load over the entire one inch face of the core plug by placing steel shot in a partial monolayer arrangement on the face of the core sample.

Figure 20 shows the resulting plot of embedment versus proppant stress generated for the Wilcox shale sample. As shown, the embedment increased linearly with proppant stress

Figure 20: Embedment Testing of the Shale Sample



from 1,000 psi up to 4,000 psi. This test showed the maximum loss in the shale to embedment at 4,000 psi was $0.0856 \text{ lbs}/\text{ft}^2$ or nearly thirty percent of a grain diameter. Similar tests with rotary sidewall core plugs of sandstone showed even less embedment $0.0144 \text{ lbs}/\text{ft}^2$ or approximately five percent of a grain diameter at 4,000 psi proppant stress.

The implications of the rotary sidewall core tests are significant. First, the "A" sand is linear elastic over the range of stresses anticipated throughout the life of the field with little evidence of ductile (permanent deformation) failure. Secondly, the static Young's Modulus in the "A" sand was determined to be 2.5×10^6 psi. Thirdly, embedment is unimportant and can be accounted for.

Finally, given the build-up and rotary sidewall core test results, the cause of the poor well performance is likely due to a limited drainage area.

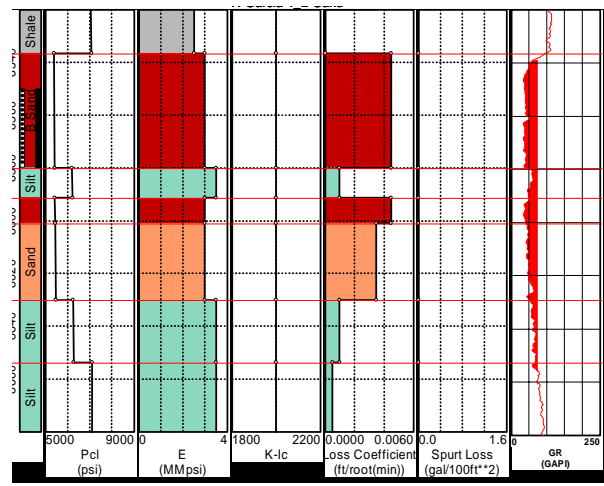
Offset Well Evaluation

Next, a preliminary fracture design was developed for the offset well completion in the "B" and possibly "A" sand. This preliminary design was constrained by the production and build-up test data on the original well and mechanical rock properties from the offset well.

Figure 21 shows a geomechanical profile developed in this manner with depth. As shown, the pressure depletion plays a major role in the in-situ stress profile in this well as the rotary sidewall core tests of static Young's Modulus (column two of

Figure 21). Further, the leak-off coefficient from the original well was used with the knowledge that pre-fracture diagnostic tests (i.e. Impulse, Step Rate, Mini-Frac Tests) were planned prior to the fracture stimulation to validate the preliminary design assumptions.

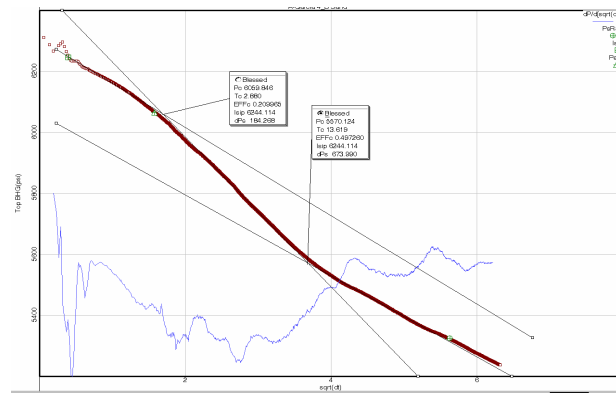
Figure 21: Constrained Geomechanical Profile- Offset Well



Preliminary Design

With the aid of the geomechanical profile with depth and a software system that couples fracture simulation and reservoir simulation with an economic model a fracture optimization study was undertaken. Based on this analysis it was determined that the optimum fracture has a half-length of 300

Figure 22: Mini-frac Square Root of Time Analysis–Offset Well



to 400 feet with good effective fracture conductivity. Additional optimization studies showed that ceramic proppant could be cost justified based on the incremental productivity, however, the use of 20/40 Ottawa sand in greater quantities resulted in optimal economics especially in light of the offset productivity issues, reservoir depletion, and poorer offset well pay quality.

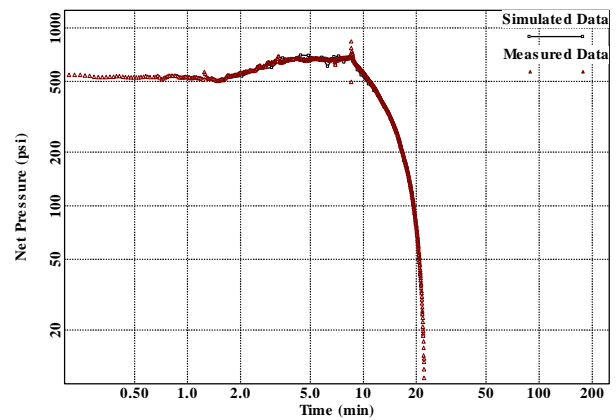
Next, the optimization study was utilized to develop a preliminary fracture design. In this manner, the offset well fracture stimulation designed was a tip screen-out design requiring a 60,000 gallon pad and 400,000 pounds of 20/40 Ottawa sand with a final in-situ proppant concentration of 5 lbs/ft².

Fracture Execution

Next, the fracturing equipment was mobilized and pre-frac diagnostic tests were conducted with bottom hole pressure gauges. The test diagnostic sequence included: (1) a small impulse injection to aid the determination of reservoir permeability, (2) a step rate test to establish fracture extension pressure (upper bound on fracture closure pressure, 6,065 psi), and (3) a mini-frac test to validate fracture closure pressure (5,570 psi) and determine the fracture fluid efficiency (0.50). Due to paper size limitations the entirety of the pre-frac diagnostic testing is not included in this paper, however, the mini-frac decline analysis is shown as Figure 22 and the mini-frac history match as Figure 23. First, a review of the mini-frac pressure decline shows some interesting character to the pressure fall-off as at least two inflection points are identified in the decline. This type of complex decline period is why one should always conduct a step –rate test because it can help establish a good upper bound on fracture closure pressure and determination of fracture closure pressure is the primary objective.

Figure 23 shows an excellent history match of net treating pressure versus time for the mini-frac that was used to modify

Figure 23: Mini-Frac Net Pressure Match-Offset Well



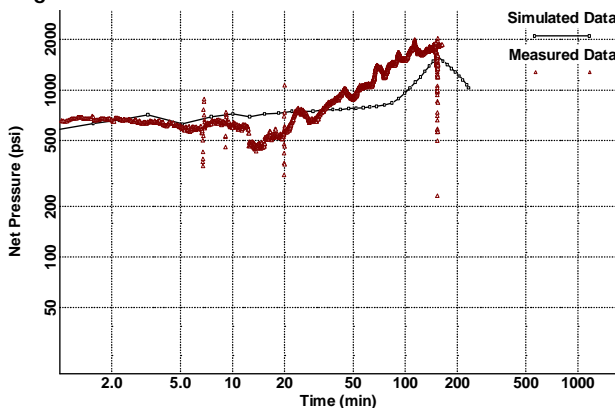
the geomechanical profile with depth used in the preliminary fracture design. Based on the net pressure history match, several modifications were made to the geomechanical profile and preliminary fracture design. These included: (1) reducing the leak-off coefficient, (2) reducing the in-situ stress contrast between the bounding beds, and (3) reduce the pad volume. These required modifications might imply the reservoir in the offset well is less permeable and that the depletion effects are less pronounced. Such findings would make the decision to utilize 20/40 Ottawa sand rather than ceramic proppant an extremely good one as the reduced permeability and tendency for additional height growth likely would result in a shorter propped fracture and an increased Dimensionless Flow Capacity over the preliminary design.

Post Fracture Evaluation

Next, the redesigned fracture treatment was pumped as designed to place 400,000 pounds of 20/40 Ottawa sand in concentrations up to 10 ppg.

Figure 24 shows the “history match” of the actual net

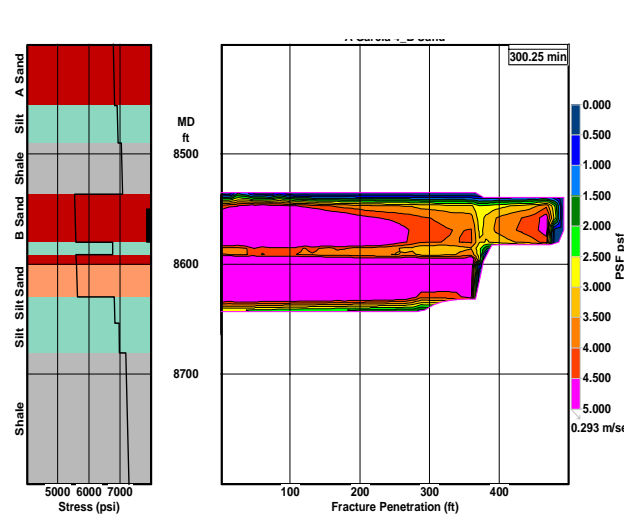
Figure 24: Frac Stimulation Net Pressure Match-Offset Well



treating pressure data as calculated from surface pressures compared to a fracture simulation prediction from the mini-frac derived geomechanical profile. As shown, a good match of the final net pressure as well as the general tip-screen-out behavior indicated that the geomechanical profile modifications made after the mini-frac was appropriate.

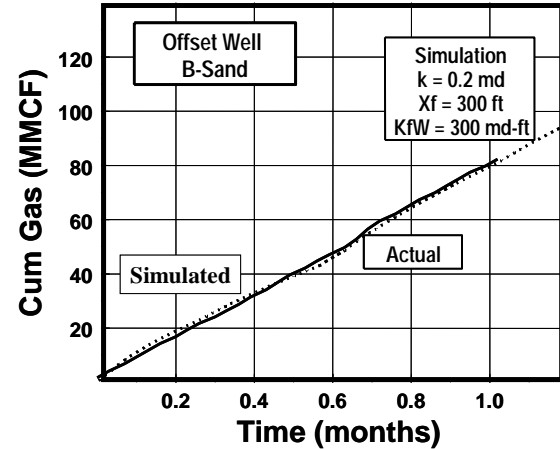
Figure 25 shows a post fracture montague comparing from left to right the final tracer profile, STIMPLAN prediction, and Gamma Ray, Neutron-Density Crossplot porosity that shows the fracture was contained to the “B” sand and sufficient fracture length, if not conductivity, were achieved for optimal or near optimal well performance. As shown, the final fracture dimensions predicted include a fracture half length of 275 to 375 feet with fracture conductivity of 5 lbs/ft². Finally, the post fracture well performance was evaluated during the first month of production. This analysis is shown in Figure 26, a plot of cumulative gas recovery versus time comparing the simulated well performance to the actual.

Figure 25: Final Post Fracture Evaluation Diagnostics for Offset Well



As shown, a good match of the production data was obtained over the first month with a reservoir permeability of 0.2 md, fracture half-length of 300 feet, and 300 md-ft of fracture conductivity. Based on this analysis, a Dimensionless Fracture Capacity, FCD, of 5.0 would result. Thus, the final placement of 400,000 pounds of 20/40 Ottawa sand resulted in a fracture two and one half times the conductivity of the optimum F_{CD} = 2. Note, that the well is still in the early stages of production, still producing water, and the fracture is still cleaning up. Therefore, the fracture conductivity and length should/may increase further with prolonged production time. One final thought, though this well made an average of 2.7 mmscfd during the first month of production as compared to the 4 to 5 mmscfd of the original well. The fracture stimulation in the offset well, was better designed, executed, and evaluated post frac because it was constrained by the rock mechanics, reservoir engineering, and leak-off data from the rotary sidewall core plugs, build-up tests, and mini-frac test,

Figure 26: Post Frac Production History Match-Offset Well



respectively. Though the original well produced at a rate 1.7 times better than the offset well, the original well had six times the flow capacity as the offset well that was fracture stimulated.

Conclusions

1. Young's modulus is an extremely important parameter to the fracturing process having nearly a direct relationship on the net treating pressure, fracture geometry, and fracture width. Since Young's modulus can be easily measured in the laboratory, it is recommended that in any area where hydraulic fracturing is used to complete and stimulate wells, core samples be taken and triaxial compression tests conducted to determine the elastic constants,
2. A Length to diameter (L/d) ratio of 1.5:1 is acceptable for geologic samples,
3. Rotary sidewall cores can be utilized for determination of elastic properties provided sample integrity is assured.

Acknowledgements

The authors wish to thank the management of BP, BP-Canada Energy Company, and Devon Energy Corporation for permission to publish this work. In addition, NSI Technologies, Inc. wishes to thank Dr. Mohan Kelkar and Tulsa University for supporting our Rock Mechanics Laboratory partnership.

Nomenclature

b_f = fracture width (ft)
 F_{CD} = Dimensionless fracture conductivity
 h = formation/fracture height (ft)
 k = formation permeability (md)
 k_f = fracture permeability (md)
 $k_f b_f$ = fracture conductivity (md-ft)
 q = total well flow rate (bopd or Mscfd)
 Q_D = Dimensionless non-Darcy flow parameter
 M = Gas Molecular weight
 x_f = fracture half-length (ft)

References

1. Boonen, P., McElhinney, G.: "Rock Mechanics and Wellbore Stability Analysis While Drilling Using LWD Sonic Density and Caliper Measurements," paper SPE/ISRM 78208 presented at the SPE/ISRM Rock Mechanics Conference held in Irving, Tx, Oct. 20-23, 2002.
2. Ringstad, C., Lothus, E.B., Sonstebo, E.F., Fjaer, E., Zausa, F., and Fuh, G.F.: "Prediction of Rock Parameters from Micro-Indentation Measurements: The Effect of Sample Size," paper SPE/ISRM 47313, presented at Eurock held in Trondheim, Norway, July, 8-10, 1998.
3. Zausa, F. and Santarelli, F.J.: "A New Method to Determine Rock Strength from an Index Test on Fragments of Very Small Dimension," VIII ISRM

International Congress on Rock Mechanics, Tokyo, Japan.

4. Santarelli, F.J., Marsala, A.F., Brignoli, M., Rossi, E., and Bona, N.: "Formation Evaluation from Logging on Cuttings," paper SPE 36851, Proc. Eur. Petroleum conf. (Milano 1996).
5. Nes, O.M., Sonstebo, E.F., Horsrud, P., and Holt, R.M.: "Dynamic and Static Measurements on mm-Size Shale Samples," paper SPE/ISRM 47200 presented at the SPE/ISRM Eurock held in Trondheim, Norway, July, 8-10, 1998.
6. Yale, D.P., Jamieson, WH: "Static and Dynamic Rock Mechanical Properties in the Hugoton and Panoma Fields, Kansas," paper SPE 27939 presented at the Mid-continent Gas Symposium held in Amarillo, Tx, May 22-24, 1994.
7. Tuman, V.S. and Alm, R.F.: "Dynamic and Static Elastic Properties of Saturated Sandstone Samples," paper SPE 603.
8. Morales, H.H., Marcin, R.P.: "Fracturing of High Permeability Formations Mechanical properties Correlations," paper SPE 26561, presented at the 68th Annual Fall Technical Conference and Exhibition held in Houston, tx, Oct. 3-6, 1993.
9. Farquhar, R.A., Somerville, J.M., and Smart, B.G.D.: "Porosity as a Geomechanical Indicator: An Application of Core and Log Data and Rock Mechanics," paper SPE 28853, presented at the European Petroleum Conference held in London, UK, Oct. 25-27, 1994.
10. Lama and Vutakuri 1978
11. Rahim, Z. and Holditch, S.A.: "The Effects of Mechanical Properties and Selection of Completion Interval Upon the Created and Propped Fracture Dimensions in Layered Reservoirs," paper SPE 24349, presented at the Rocky Mountain Regional Meeting held in Casper, Wyoming, May 18-21, 1992.
12. Smith, M.B., Rosenburg, R.J. and Bowen, J.F.: "Fracture Width - Design Versus Measurement," paper SPE 10965 presented at the 57th Annual Fall Technical Conference and Exhibition held in New Orleans, LA, Sept. 26-29, 1982.
13. Lacy, L.L.: "Dynamic Rock Mechanics Testing for Optimized Fracture Designs," paper SPE 38716, presented at the 1997 Annual Fall Technical Conference and Exhibition held in San Antonio, TX, Oct. 5-8, 1997.